Optical Materials 140 (2023) 113910

Contents lists available at ScienceDirect

Optical Materials

journal homepage: www.elsevier.com/locate/optmat

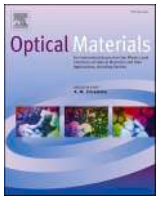

Research Article

Spectroscopic studies of Pr^{3+} doped red-emitting BaO–ZnO– Li_2O–P_2O_5 glasses for luminescent devices applications

Kartika Maheshwari [a,b], Ravita [c], Aman Prasad [d], Yasha Tayal [a,b], A.S. Rao [a,*]

[a] Department of Applied Physics, Delhi Technological University, Bawana Road, Delhi, 110042, India
[b] ABES Engineering College, Ghaziabad, 201 009, India
[c] Department of Physics, Chaudhary Bansi Lal University, Bhiwani, 127021, India
[d] Department of Physics and Computer Science, Dayalbagh Educational Institute (DEI), Agra, 282005, India

ARTICLE INFO

Keywords:
Glasses
Luminescence
Decay kinetics
J-O Theory
Activation energy

ABSTRACT

Pr^{3+} doped BaO–ZnO– Li_2O–P_2O_5 (BZLP) glass samples synthesised through melt quenching route were studied. The x-ray diffraction (XRD) confirms the amorphous non-crystalline nature of undoped and doped BZLP glass. Absorption spectra show several bands in ultraviolet, visible and infrared regions. The absorption data was used in Judd-Ofelt (J-O) theory to evaluate various radiative parameters. Three peaks are visible in the photoluminescence (PL) emission spectra with the strongest peak positioned at 604 nm for which stimulated emission cross section and quantum efficiency has been assessed. The CIE color coordinates of the samples lie in the red region. The decay time values for 604 nm emission decreased with increased Pr^{3+} concentration. The luminescence intensity decreased to 88.12% and 82.61% of maximum value at 423 K and 473 K respectively showing high thermal stability. These BZLP glasses can work as an effective deep red-emitting component for w-LEDs and other photonic applications.

1. Introduction

Lighting is one of the most fundamental and essential parts of our everyday lives. A variety of electricity-based artificial lighting technologies are available and are being used for indoor/outdoor illumination and lighting industries, complexes, and other areas [1,2]. Solid-state lighting (SSL) technology is one of the advanced artificial lighting technologies. It is eco-friendly in nature and more efficient thereby saving enormous energy in various sectors [3,4]. The white light emitting diodes (w-LEDs) are most widely researched amongst all SSL devices. w-LEDs are developed by mixing a yellow color emitting phosphor with an inorganic compound (epoxy resin) and coated over a blue InGaN chip [5]. This technique has some shortcomings likee less color rendering index, inappropriate correlated color temperature and a halo-effect owing to absence of a red color component. To overcome the drawbacks as mentioned above, numerous other approaches were explored and published [3,6]. These approaches involved usage of inorganic phosphors having less thermal stability, which reduced efficiency and performance of illuminating devices [7]. Therefore, a suitable glass doped with an appropriate lanthanide/transition metal ions is the best replacement for a phosphor. So, in this work, thermally stable red-emitting inorganic glasses were synthesised and explored for lighting applications.

Inorganic oxide formers like phosphates are used to prepare excellent glasses for usage in numerous applications due to eco-friendliness, high transparency, ease of synthesis, low preparation cost, better mechanical and thermal stability etc. [8,9]. Also, high transparency in ultraviolet (UV) to infrared (IR) regions and high rare-earth solubility make phosphates a superior glass host material for photonic applications as compared to borate and silicate glasses [10,11]. But phosphate glass are hygroscopic in nature, which restricts their utility in many applications. The hygroscopic nature of phosphate glasses can be tackled by adding ZnO, which constitutes P–O–Zn bonds and makes the glass moisture resistant [12,13]. Also, the addition of ZnO offers superior characteristics like direct bandgap, non-toxicity, less cost, non-hygroscopic and large exciton binding energy [14]. Alkaline earth metal oxide can work as an active network modifier, which can disrupt the glass network thereby leading to creation of nonbridging oxygen groups and bringing down the melting temperature of glass compositions [15,16]. The addition of alkali oxide in glass compositions may reduce the non-radiative losses, heighten the stability of host matrix. Addtion of lithium oxide to the host leads to the intensification of

* Corresponding author.
E-mail address: drsrallam@gmail.com (A.S. Rao).

https://doi.org/10.1016/j.optmat.2023.113910
Received 5 April 2023; Received in revised form 9 May 2023; Accepted 15 May 2023
Available online 23 May 2023
0925-3467/© 2023 Elsevier B.V. All rights reserved.

transition temperature and lowering of thermal expansion coefficient [17]. With aforementioned characteristics in mind, we were able to synthesize BaO–ZnO–Li_2O–P_2O_5 (BZLP) glass that is highly transparent, moisture-resistant, has less phonon energy, is thermally and mechanically stable with excellent optical characteristics.

Lanthanide ions exhibit a ladder like energy level structure in the ultraviolet (UV) to infra-red (IR) range which is extremely useful for lasing and other photonic device applications [18,19]. The radiative emissions in the lanthanide ions are due to the f-f transitions of 4f shells that are screened by the $5s^2/5p^6$ orbitals [17,20]. Europium, praseodymium and samarium ions in trivalent states produce radiative emission in orange/red regions via pumped by UV/near-UV/blue radiations [21]. Among these lanthanides, Pr^{3+} ions can effectively absorb blue emission emanating from blue LED chips and has significant fluorescence emission in the conspicuous deep-red range of the electromagnetic spectrum [22,23].

In this work, various optical and morphological characteristics of highly transparent Pr^{3+} doped BZLP glass samples have been examined in detail. Absorption data was used to determine the bandgap of the as prepared glass. Photoluminescence (PL) excitation and emission studies were conducted on the glass samples. Under 445 nm excitation, the glasses show a sharp band centered at 604 nm. Decay curves for 604 nm emission were plotted as well. Temeperature dependent PL studies were performed to check whether or not the samples are thermally stable. The aim of performing all the aforementioned studies was to check the applicability of Pr^{3+} glass in w-LEDs and SSL applications.

2. Experimental work and characterizations

2.1. Preparation of glass

Trivalent praseodymium (Pr^{3+}) doped glass samples were synthesised by employing melt quenching route. The doped and undoped glass samples have the molar configuration as follows:

$$(15 - x)\ BaO - 15ZnO - 10Li_2O - 60P_2O_5 : xPr_6O_{11}$$

In the above-mentioned molar composition, *x* represents the amount of Pr^{3+} ions in BZLP glasses. In this study, x varies as 0.0, 0.01, 0.05 0.1, 0.5, 1.0, 1.5, 2.0 & 2.5 mol% and the glasses have been assigned names as BZLP, BZLP:0.01Pr, BZLP:0.05Pr, BZLP:0.1Pr, BZLP:0.5Pr, BZLP:1.0Pr, BZLP:1.5Pr, BZLP:2.0Pr and BZLP:2.5Pr respectively.

Annular grade precursors and 99.9% pure rare earth materials were employed to prepare undoped and Pr^{3+} doped glass samples. The raw chemical powders were weighed as per the composition calculation. The chemicals were ground using the agate mortar and pestle with ethanol as dispersing medium for 1 h. Then, this homogenous and smooth chemical mixture was transferred to an alumina crucible and heated in a muffle furnace from room temperature till 1150 °C at a rate of 5 °C per minute and a hold at 1150 °C for 1 h. This homogeneous melt mix was then taken out and swiftly pressed between preheated (320 °C) brass plates to form glass of desired shape and thickness. To eradicate bubbles and thermal strain, the prepared glass was annealed at 320 °C for 1 h. Finally, the undoped and Pr^{3+} doped BZLP glass samples were ready for the structural, optical and other characteristations.

2.2. Characterization techniques

The physical characteristics for Pr^{3+} doped BZLP glass samples such as density and refractive index and other related parameters were assessed using Archimedes principle (H_2O used as a measuring medium) and He–Ne laser (650 nm). Diffraction patterns of undoped and Pr^{3+} doped BZLP glass samples were recorded at room temperature (300 K) via Bruker D8 Advance X-Ray diffractometer attached with a Ni filter and Cu (K_α) radiation source in $20^\circ \leq 2\theta \leq 70^\circ$ range. Using a spectrophotometer JASCO V 670, optical absorption spectral investigations were measured in the UV to near-infrared (NIR) range.The photoluminescence studies for Pr^{3+} doped BZLP glass samples were carried out via spectrofluorophotometer JASCO 8300FL at 300 K. Decay profile for Pr^{3+} doped BZLP glass samples were recorded via EdinburgFLS980 coupled with a microsecond Xenon flash lamp. Temperature-dependent photoluminescence (TD-PL) features were observed with FLAME- S-XR1-ES Ocean optics spectrophotometer and sample holder attached with heating assembly.

3. Results and discussion

3.1. Physical properties of Pr^{3+} doped BZLP glass samples

The density and refractive index of the samples were calculated using Archemedes' principle and Brewster's angle method respectively [24]. Other related physical parameters were also calculated using formulae from relevant articles in literature and have been presented in Table 1 [25].

The physical parameters for Pr^{3+} doped BZLP glass samples showed variation with an increase in Pr^{3+} ions concentration due to altered environment around the Pr^{3+} ions. The values of parameters like molar refraction, average molecular weight, optical dielectric constant, molar refraction and reflection losses were seen to be increasing with increase in the Pr^{3+} ions concentration in BZLP glass samples whereas polaron radius and interatomic distance decreased with increasing Pr^{3+} ions.

3.2. Glass structural analysis

Diffraction patterns for BZLP and BZLP:0.1Pr glass samples have been recorded at room temperature and shown in Fig. 1. The spectra shows a broad ranging hump and absence of any sharp peaks thereby confirming the amorphous nature of the glass. Also, the doping of Pr^{3+} ions in BZLP glass does not affect the amorphous properties of the doped glasses.

3.3. Absorption properties of glass

Fig. 2 shows the absorption spectra from UV to IR region for BZLP glasses doped with Pr^{3+} ions that were measured at room temperature. The absorption profile exhibits numerous peaks in 300–2000 nm wavelength range. In the spectra, three peaks related to $^3H_4 \rightarrow {}^3P_{2,\ 1,\ 0}$ transitions and one peak related to $^3H_4 \rightarrow {}^1D_2$ transition is present in the visible range and the residual three peaks were related to $^3H_4 \rightarrow {}^1G_4$, $^3F_{4,3,2}$ transitions present in NIR region [26]. These transitions are in agreement with Carnall's work [27]. The absorption intensity increased with increase in the concentration of Pr^{3+} ions. The $^3H_4 \rightarrow {}^3P_2$ transition is hypersensitive in nature [$|\Delta S| = 0, |\Delta L| \leq 2$ *and* $|\Delta J| \leq 2$] which predominantly depends upon on the neighbourhood of Pr^{3+} ions and correspondingly affects the J-O intensity parameters [28]. The hypersensitive transition's peak position is shifted towards shorter wavelengths as depicted in Fig. 2 when the concentration of Pr^{3+} ions rises. This change in shift arises due to nephelauxetic effect [29]. For the mentioned band positions in absorption spectra, nephelauxetic ratio (β and bonding parameters (δ) were assessed for Pr^{3+} doepd BZLP glasses by employing expression in literature [29,30]. Bonding parameters can represent the covalent or ionic character of as-prepared glasses by having + ve or -ve values respectively. Table 2 shows that the bonding parameter values are positive, indicating the covalent character of as prepared glasses. This covalent nature increases in the as prepared glasses as the concentration of Pr^{3+} ions rises.

An essential parameter, the experimental oscillator strength (fexp), has been evaluated using the area under the absorption peaks and applying the specified formula:

$$f_{exp} = \frac{2.303mc^2}{N\pi e^2} \int \varepsilon(\vartheta) d\vartheta \quad (1)$$

Table 1
Physical Properties of Pr^{3+} doped BZLP glasses.

Physical Property	BZLP: 0.01Pr	BZLP: 0.05Pr	BZLP: 0.10Pr	BZLP:0.50Pr	BZLP:1.00Pr	BZLP:1.50Pr	BZLP:2.00Pr	BZLP:2.5Pr
Refractive index (n_d)	1.78	1.81	1.84	1.86	1.89	1.93	1.94	1.96
Density (gm/cm^3)	2.99	3.09	3.14	3.18	3.20	3.22	3.26	3.28
Average molecular weight	208.61	208.96	209.39	212.86	217.20	221.54	225.89	230.23
Pr^{3+} ion concentration N (10^{22} ions/cm^3)	0.008	0.04	0.09	0.45	0.88	1.32	1.73	2.14
Polaron radius (r_p) (Å)	9.10	5.27	4.16	2.43	1.94	1.70	1.55	1.44
Inter-atomic distance (r_i) (Å)	22.60	13.09	10.33	6.05	4.82	4.23	3.85	3.59
Optical band gap (eV)	3.57	3.51	3.48	3.64	3.92	3.94	4.02	4.07
Dielectric constant (Ɛ)	3.16	3.27	3.38	3.45	3.57	3.72	3.76	3.84
Optical dielectric constant (Ɛ-1)	2.16	2.27	2.38	2.45	2.57	2.72	2.76	2.84
Molar refraction (R_m) (cm^{-3})	29.18	29.14	29.45	30.10	31.30	32.67	33.19	34.09
Reflection losses (R %)	4.25	4.51	4.78	4.96	5.23	5.59	5.69	5.87

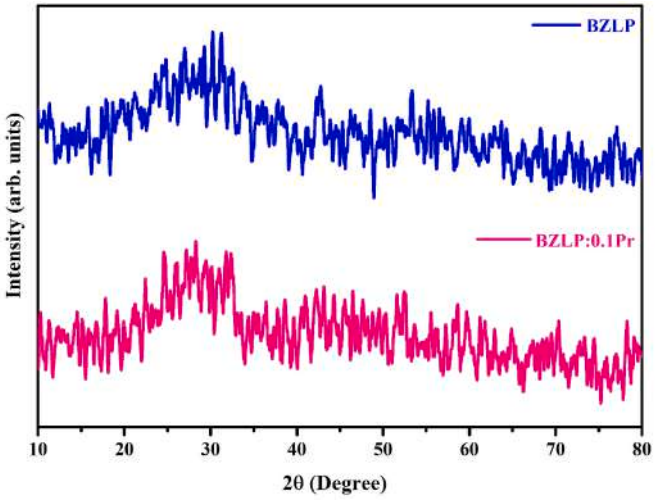

Fig. 1. XRD patterns recorded for BZLP and BZLP:0.1Pr glasses.

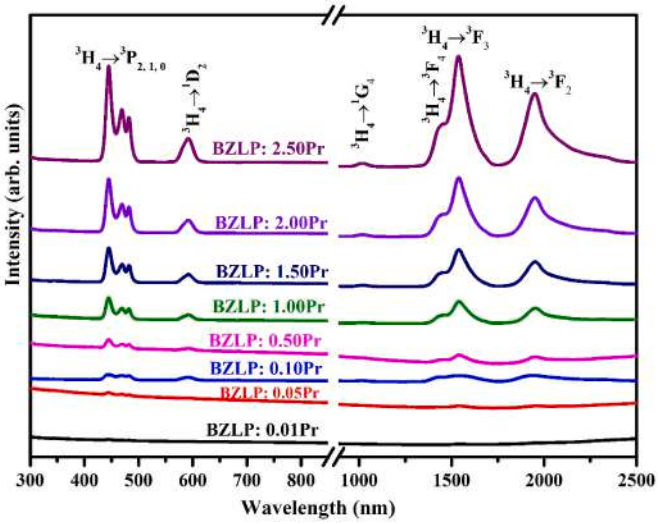

Fig. 2. Absorption spectra of doped BZLP glasses with varying concentrations of Pr^{3+} from 0.01 to 2.5 mol%.

where m, e, and c denotes for mass, charge of an electron and speed of light respectively. Also, N here stands for the Avagadro's Number, while $\varepsilon(\vartheta)$ is the molar extinction coefficient for the wave number ϑ (cm^{-1}.) The evaluated values are have been presented in Table 2. The calculated oscillator strength (f_{cal}) and J-O parameters (Ω_2, Ω_4, Ω_6) were estimated through experimental oscillator strength (f_{exp}). Least square fit method is used to evaluate the calculated oscillator strength for measured electric dipole transitions within $4f^2$ configuration using following relevant equation:

$$f_{cal} = \left[\frac{8\pi^2 mcv}{3h(2J+1)}\right]\left[\frac{(n^2+1)^2}{9n}\right]\sum_{\lambda=2,4,6}\Omega_\lambda\left(\Psi J \parallel U^\lambda \parallel \Psi' J'\right)^2 \quad (2)$$

Where, ϑ is the wave number for ground state (φ_J) to excited state $(\varphi_{J'}^{i})$ transition, m is electron's mass, c is the speed of light in free space and $\|U^\lambda\|^2$ is doubly reduced matrix element. The best fit between f_{exp} and f_{cal} is assessed through the root mean square deviation (δ_{rms}) that can be calculated by employing the subsequent formula:

$$\delta_{rms} = \left[\frac{\sum\left(f_{exp} - f_{cal}\right)^2}{N}\right]^{\frac{1}{2}} \quad (3)$$

Here N represents the overall number of peaks used in the fitting. The values of f_{cal}, f_{exp}, and δ_{rms} for BZLP glasses are shown in Table 2. Table 3 lists the evaluated J-O intensity parameters together with the values of other reported glasses from the literature [31–34]. J-O parameters emulate the uniform trend ($\Omega_4 > \Omega_2 > \Omega_6$) for all reported glass samples. The intensity parameter Ω_2 is a depiction of covalent character of metal ligand bond whereas other two parameters Ω_4 and Ω_6 indicate the rigidity and viscosity of host glass matrix. The Ω_2 parameter of the BZLP 0.1Pr glass is greater than those of the earlier reported glasses [31,32,35–37] and is comparable to those of Pr^{3+}doped ZnAlBiB glasses reported by Mahamuda et al. [26]. The higher value of Ω_2 parameter observed for BZLP 0.1Pr glass implies a greater degree of covalency of the Pr^{3+} ions bonding with the oxygen ligand, which is verified by the bonding parameters listed in Table 2 and may also be an indication of a greater degree of asymmetry in the ion sites around the Pr^{3+} ions. In contrast, higher value of Ω_4 implies more rigidty of host medium around the Pr^{3+} ions [38,39]. For the present glass system, J-O intensity parameter Ω_4 increases as the concentration of Pr^{3+} ions rises from BZLP:0.01Pr to BZLP:0.1Pr and then decreases up to BZLP:2.5Pr. Greater the value of Ω_4 intensity parameter for prepared glasses indicates the rigidty of host material in which Pr^{3+} ions are located [26].

The optical band gap is a vital parameter and was calculated for Pr^{3+} ions doped BZLP glass samples based on recorded absorption spectra. According to Davis and Mott's relation, the optical band gap for glass samples was estimated through the following relation [14]:

$$\alpha(\nu) = \left(\frac{B}{h\nu}\right)\left(h\nu - E_{opt}\right)^n \quad (4)$$

here, $h\nu$ denotes the incident photon energy, E_{opt} signifies the optical energy band gap, B stands for the band tailing parameter, n is an index number.The type of transition depends on the value of parameter n. For direct and indirect permissible transitions, the prescribed values are $n =$ ½ and $n = 2$ respectively. The value of $\alpha(\nu)$ was estimated using the following expression [40]:

Table 2
Experimental (f_{exp}) (x10^{-6}), calculated (f_{cal}) (x10^{-6}) oscillator strengths, r.m.s deviation (δ_{rms}), nephelauxetic ratio ($\bar{\beta}$), and bonding parameters (δ) for Pr^{3+} ions in BZLP glasses.

Transitions from $^3H_4$→	BZLP:0.01Pr		BZLP:0.05Pr		BZLP:0.1Pr		BZLP:0.5Pr		BZLP:1.0Pr		BZLP:1.5Pr		BZLP:2.0Pr		BZLP:2.5Pr	
	f_{cal}	f_{exp}	f_{exp}	f_{cal}	f_{exp}	f_{cal}	f_{exp}	f_{cal}	f_{exp}	f_{cal}	f_{exp}	f_{cal}	f_{exp}	f_{cal}	f_{exp}	f_{cal}
$^3F_2$	4.76	4.73	5.79	5.76	9.73	9.72	5.74	5.75	4.21	4.22	4.09	4.11	3.95	3.98	3.73	3.76
$^3F_3$	6.05	6.31	6.83	7.18	10.4	10.3	6.89	6.50	5.55	5.22	5.12	4.70	4.67	3.99	4.56	3.83
$^3F_4$	–	–	3.5	3.64	3.65	5.05	1.87	3.18	1.63	2.55	1.43	2.30	0.37	1.65	0.21	1.56
$^1D_2$	–	–	8.77	1.17	12.8	1.65	5.86	1.04	4	0.84	2.78	0.75	2.67	0.60	2.63	0.581
$^3P_0$	5.72	5.18	6.03	3.94	6.54	5.94	2.36	3.79	1.93	3.15	1.32	2.75	1	3.13	0.78	3.10
$^3P_1$	–	–	2.29	4.01	2.66	6.04	2.3	3.86	2.22	3.21	1.93	2.80	1.81	3.19	1.77	3.16
$^3P_2$	7.61	3.05	7.75	3.71	12.9	5.14	9.28	3.27	5.9	2.65	4.04	2.36	3.88	1.84	3.7	1.76
δ_{rms} (x 10^{-6})	2.29		3.41		5.34		3.06		1.85		1.23		1.55		1.58	
$\bar{\beta}$	0.997		0.995		0.994		0.993		0.998		0.998		0.997		0.997	
δ	0.03		0.05		0.06		0.07		0.12		0.15		0.20		0.21	
																0.2115

Table 3
Judd-Ofelt Parameters ($\Omega_i \times 10^{-20} cm^2$) of Pr^{3+} ions in BZLP glasses along with various reported hosts.

Glass System	Ω_2	Ω_4	Ω_6	Trend	References
BZLP: 0.01Pr	2.57	5.20	3.05	$\Omega_4 > \Omega_2 > \Omega_6$	Present work
BZLP: 0.05Pr	5.34	5.40	4.47	$\Omega_4 > \Omega_2 > \Omega_6$	Present work
BZLP: 0.1Pr	7.86	9.98	5.88	$\Omega_4 > \Omega_2 > \Omega_6$	Present work
BZLP: 0.5Pr	4.94	5.45	3.67	$\Omega_4 > \Omega_2 > \Omega_6$	Present work
BZLP: 1.0Pr	3.48	4.00	2.87	$\Omega_4 > \Omega_2 > \Omega_6$	Present work
BZLP: 1.5Pr	3.23	3.38	2.50	$\Omega_4 > \Omega_2 > \Omega_6$	Present work
BZLP: 2.0Pr	3.03	3.22	1.61	$\Omega_4 > \Omega_2 > \Omega_6$	Present work
BZLP: 2.5Pr	2.87	3.72	1.48	$\Omega_4 > \Omega_2 > \Omega_6$	Present work
$(Ge_{30}Ga_5Se_{65})_{100-x}$ $(Pr_2 Se_3)x$	6.00	16.8	5.00	$\Omega_4 > \Omega_2 > \Omega_6$	[31]
$59.99TeO_2$ –$25WO_3$ – $15PbF_2$ – $0.01Pr_6O_{11}$	4.782	6.148	2.208	$\Omega_4 > \Omega_2 > \Omega_6$	[32]
TeWLiK	8.56	9.64	2.80	$\Omega_4 > \Omega_2 > \Omega_6$	[33]
TeWNaK	9.39	9.55	2.81	$\Omega_4 > \Omega_2 > \Omega_6$	[33]
Phosphate	4.19	4.29	6.40	$\Omega_6 > \Omega 2 > \Omega_4$	[35]
Mixed halide	2.70	4.40	5.40	$\Omega_6 > \Omega 2 > \Omega_4$	[36]
ZnAlBiB 1.0Pr	7.36	4.46	4.17	$\Omega_2 > \Omega 4 > \Omega_6$	[26]
ZBP5	3.94	1.34	1.23	$\Omega_2 > \Omega_4 > \Omega_6$	[37]
$40GaS_{3/2}$.$40GeS_2$.20Cs	9.05	7.26	7.28	$\Omega_2 > \Omega_6 > \Omega_4$	[34]

$$\alpha(\nu) = \left(\frac{1}{d}\right) ln\left(\frac{I_0}{I_T}\right) \quad (5)$$

Here, the thickness of glass denotes by d. The absorbance varies by a factor of $ln\,(I_0/I_T)$. The E_{opt} values were acquired for indirect allowed transitions by extrapolating the linear section of the Tauc's plot [$(ah\nu)^{1/n}$ versus $(h\nu)$] as presented in Fig. 3 with $n = 2$. The estimated bandgap E_{opt} values for Pr^{3+} ions doped BZLP glass samples have been listed in Table 1 and lie in the range 3.48–4.07 eV.

3.4. PL characteristics of glass

PL excitation spectrum of BZLP1.0Pr glass sample was recorded in 400–500 nm range with monitoring emission wavelength $\lambda_{em} = 604$ nm and has been presented in Fig. 4. Three excitation peaks ascribed to $^3H_4 \rightarrow {}^3P_2$, $^3P_1$,$^3P_0$ transitions of Pr^{3+} ions, respectively can be seen. The most intense excitation was seen at 445 nm corresponding to $^3H_4 \rightarrow {}^3P_2$ transition and this was selected for recording the photoluminescence emission spectra of all prepared glass samples at room temperature [27].

The PL emission spectra of Pr^{3+}doped BZLP glasses at $\lambda_{ex} = 445$ nm have been presented in Fig. 5. Emission peaks were noticed at 604, 616 and 647 nm corresponding to $^1D_2 \rightarrow {}^3H_4$, $^3P_0 \rightarrow {}^3H_6$ and $^3P_0 \rightarrow {}^3F_2$ transitions of Pr^{3+} ions respectively. Among the emission peaks, the dominant one is due to $^1D_2 \rightarrow {}^3H_4$ transition at 604 nm. In the emission spectra ranging between 600 and 620 nm, emission bands ($^1D_2 \rightarrow {}^3H_4$ and $^3P_0 \rightarrow {}^3H_6$) are observed, which are overlapped in proximity. The peak observed in the red region: $^3P_0 \rightarrow {}^3H_6$ has better sharpness as the concentration of Pr^{3+} ions is increased beyond 0.5 mol% while $^1D_2 \rightarrow {}^3H_4$ transition loses its sharpness at this concentration. The band maxima shifts from 604 nm to 616 nm as the concetration of dopant ion is increased [41–43]. The intensity of the peaks increased with increase in Pr^{3+} ions content up 0.1 mol% and decreased afterwards. This is due to concentration quenching. This occurs as soon as the interionic distance among the Pr^{3+} ions becomes lesser than the critical distancei.e the minimum distance between two doping ions. In this condition, the energy migration amongst dopant Pr^{3+} ions happens via radiationless transfer either by multiphonon or cross-relaxation process [44].The inset plot of Fig. 5 demonstrates the change in PL intensity with concetration of Pr^{3+} ions in BZLP glasses.

The excitations, non-radiative and radiative emissions of Pr^{3+} ions in BZLP glass and cross-relaxation channels (CRC) were well clarified by the energy level diagram as demonstrated in Fig. 6. The energy level diagram shows the absorption of specific energy and subsequently movement of ions from the ground state to a specific excited state. After a certain time, the excited ions return to the ground level via radiationless and radiative emissions. As per the energy of presented levels of Pr^{3+}, the possible CRC responsible for the concentration quenching are as below [26]:

CRC 1: $^3P_0 + {}^3H_4 \rightarrow {}^1D_2 + {}^3H_6$

CRC 2: $^3P_0 + {}^3H_4 \rightarrow {}^3H_6 + {}^1D_2$

CRC 3: $^3P_0 + {}^3H_4 \rightarrow {}^1G_4 + {}^1G_4$

The non-radiative energy transfer takes place in rare-earth-doped luminescent materials due to the multipolar interaction among dopant ions. Dexter theory predicts three kinds of mechanisms for interionic multipolar interactions between the dopant ions. As per the theory the PL intensity is related to the amount of doping ion content in the host system as [45]:

$$log\left(\frac{I}{c}\right) = logf - \frac{s\,log(c)}{d} \quad (6)$$

here I denotes the PL intensity, c is the Pr^{3+} ion concentration in BZLP glass samples, d denotes the dimension of the compound having the value of $d = 3$. f signifies a constant, which is unaffected by doping ion concentration. The parameter s describes the type of multipolar

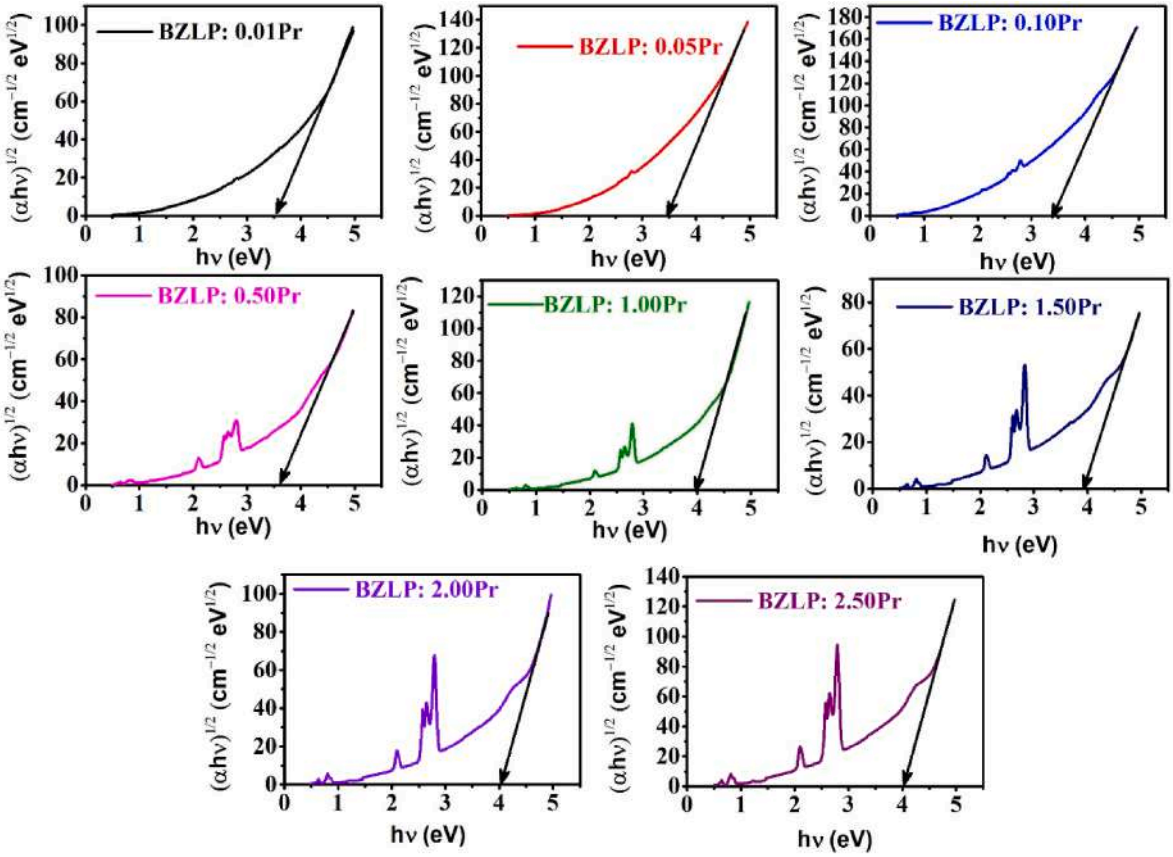

Fig. 3. Indirect bandgap plot of Pr^{3+} doped BZLP glasses with varying concentration from 0.01 to 2.50 mol%.

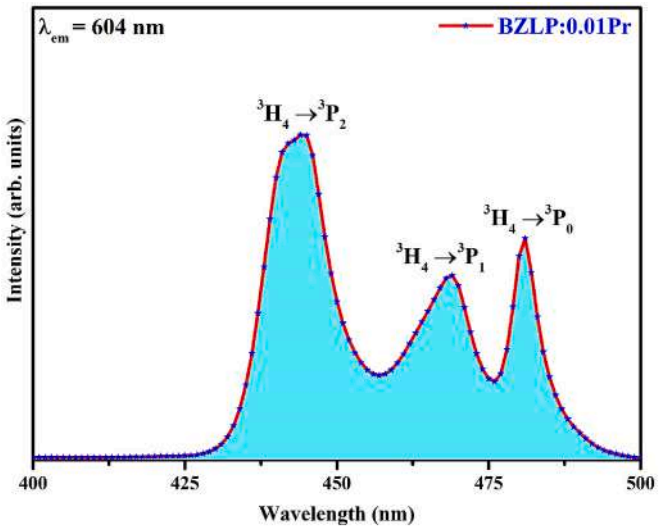

Fig. 4. The excitation spectrum recorded for BZLP:0.01Pr glass under 604 emission wavelength.

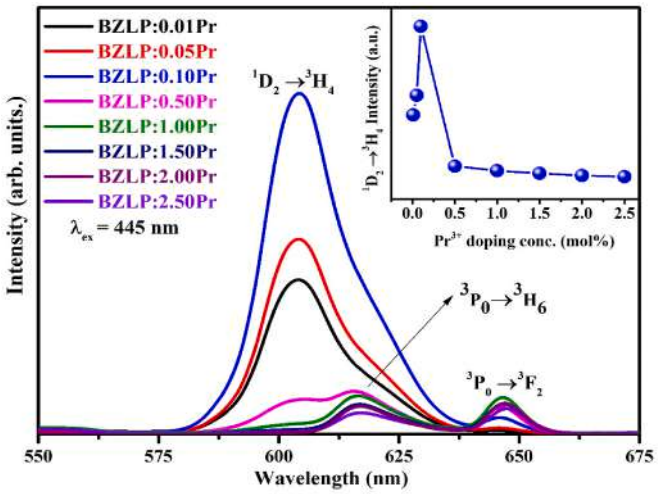

Fig. 5. Emission spectra of Pr^{3+} doped BZLP glasses with varying the doping concentration from 0.01 to 2.50 mol%. Inset plot shows the variation of the emission intensity related to $^1D_2 \rightarrow {}^3H_4$ transition with Pr^{3+} ions concentration.

interaction within the adjacent Pr^{3+} ions in BZLP glass samples. The value of parameter *s* is 6 for dipole-dipole interaction, 8 for dipole-quadrupole inetraction and 10 for quadrupole-quadrupole multipolar interaction [16]. For this research work, the value of parameter *s* was estimated using the slope of the linear fitted plot of $log\ (I/c)$ versus $log(c)$ as shown in Fig. 7 and was found to be 1.485. Therefore the estimated value of parameter *s* was 4.455 which is close to 6. This proves that the non-radiative multipolar interaction between the Pr^{3+} ions is dipole-dipole in nature. In accordance with Dexter Theory, the emission and absorption spectrum of doped glasses will overlap. The visible range emission and absorption spectrum of the $^1D_2$ transition, as well as the cross relaxation channel overlap as shown in Fig. 8 [44]. This spectral overlap enables us to comprehend the resonant energy transfer between excited and unexcited Pr^{3+} ions.

The photoluminescence performance for Pr^{3+} doped BZLP glasses is estimated by calculating the parameters like radiative transition probability (A_R), total transition probability (A_T),radiative lifetime (τ_R) and

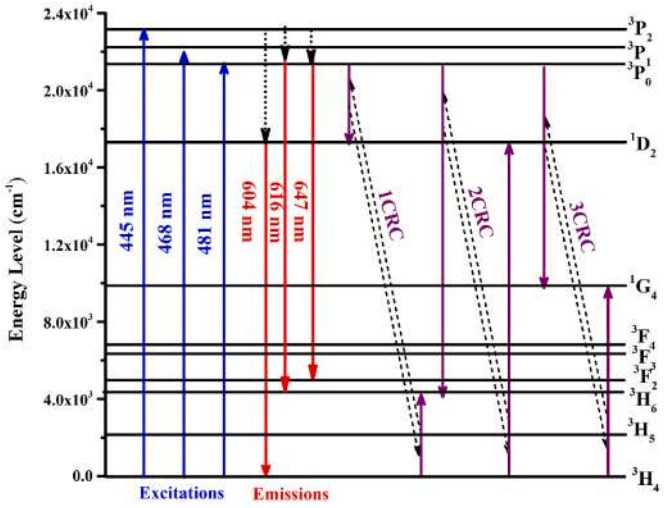

Fig. 6. Energy level diagram of Pr^{3+} doped BZLP glasses.

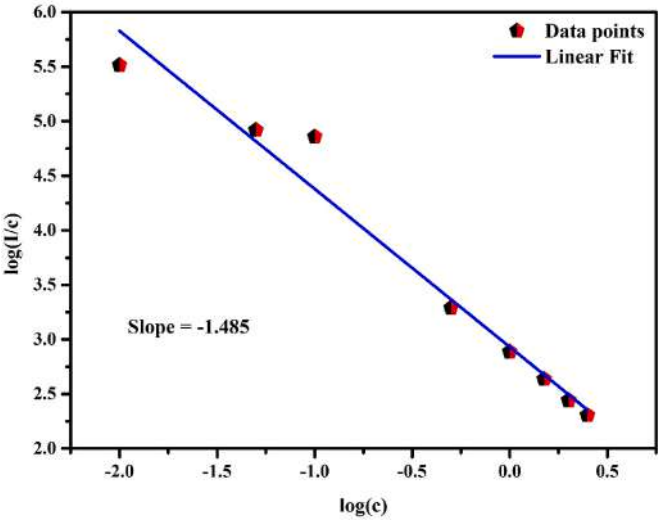

Fig. 7. Relation between log (I/c) and log (c) for different concentrations of Pr^{3+}.

luminescence branching ratio (β_R) with the aid of J-O intensity parameters measured from the absorption spectra. These parameters have been listed in Table 3. To explore the luminescent process, the radiative transition probability (A_R) for flouroscent levels can be computed by using the following equation [46]:

$$A_R(a_J, b_{J'}) = \frac{64\pi^4 \vartheta}{3h(2J+1)}\left[\frac{n(n^2+2}{9} s_{ed}(a_J, b_{J'}) + n^3 S_{md}(a_J, b_{J'})\right] \quad (7)$$

The total transition probability (A_T) for flouroscent levels can be computed by using the following equation [46]:

$$A_T = \sum_{b_{J'}} A_R(a_j, b_{j'}) \quad (8)$$

The radiative lifetime $\tau_R\ (a_j, b_{j'})$ and the luminescence branching ratio $\beta_R\ (a_j, b_{j'})$ from a ground state a_j to an excite state $b_{j'}$ are given by [46]:

$$\tau_R(a_j, b_{j'}) = \frac{1}{\sum_{b_{j'}} A_R(a_j, b_{j'})} \quad (9)$$

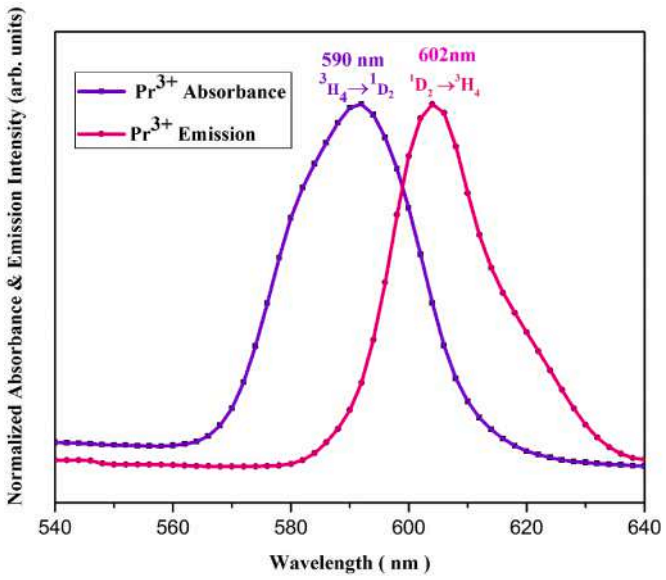

Fig. 8. Spectral overlap of absorbance & emission spectrum of BZLP:0.1 glass for transition $^1D_2 \rightarrow {}^3H_4$.

$$\beta_R\ (a_j, b_{j'}) = A_R(a_j, b_{j'}).\tau_R(a_j, b_{j'})$$

An essential parameter is stimulated emission cross-section (σ_{se}) and its value dictates high gain and low threshold for lasing applications. It is given by the following expression [46,47]:

$$\sigma_{se} = \frac{\lambda_p^4}{8\pi c n^2 \Delta\lambda_p} A_R \quad (10)$$

Where λ_p represents the peak wavelength, $\Delta\lambda_p$ is the effective width of the emission transition and c, n and A_R symbolize speed of light in free space, refractive index and radiative transition probability of flouroscent levels respectively.

A_R, A_T, β_R and τ_R radiatitve parameters computed for Pr^{3+} doped BZLP glasses for all fluoroscent transitions are listed in Table 4. Other radiative parameters like λ_p (peak wavelength), $\Delta\lambda_p$ (effective band width), β_R, β_{exp} (radiative and experimental brnching ratio) , σ_{se}(stimulated emission cross section), σ_{se} x $\Delta\lambda p$ (gain bandwidth) and σ_{se} x τ_R (optical gain parameters) are represented in Table 5 for all reported glasses. Fluoroscent Branching ratio (β_R) is another significant parameter for lasing action and its value should be around 0.5. From Tables 5

Table 4
Transition probability (A_R) (s^{-1}), luminescence branching ratio (β_R), total transition probability (A_T) (s^{-1}) and radiative lifetime (τ_R) (μs) for the observed emission transitions of Pr^{3+} ions in BZLP glass.

Sample name	Transition	A_R	A_T	β_R	τ_R
BZLP: 0.01Pr	$^3P_1 \rightarrow {}^3F_3$	10071.61	48833.47	0.2062	20
	$^1D_2 \rightarrow {}^3H_4$	978.62	3947.08	0.2479	253
BZLP: 0.05Pr	$^3P_1 \rightarrow {}^3F_3$	17721.88	66333.76	0.2672	15
	$^1D_2 \rightarrow {}^3H_4$	1372.52	6371.21	0.2154	156
BZLP: 0.1Pr	$^3P_1 \rightarrow {}^3F_3$	32900.21	110698.7	0.2972	9
	$^1D_2 \rightarrow {}^3H_4$	2001.65	11082.17	0.1806	90
BZLP: 0.5Pr	$^3P_1 \rightarrow {}^3F_3$	19264.42	68643.08	0.2806	14
	$^1D_2 \rightarrow {}^3H_4$	1293.03	6665.77	0.194	150
BZLP: 1.0Pr	$^3P_1 \rightarrow {}^3F_3$	13848.99	54324.4	0.2549	18
	$^1D_2 \rightarrow {}^3H_4$	1073.6	5003.91	0.2146	199
BZLP: 1.5Pr	$^3P_1 \rightarrow {}^3F_3$	13504.31	51079.94	0.2644	19
	$^1D_2 \rightarrow {}^3H_4$	1000.98	4811.39	0.208	207
BZLP: 2.0Pr	$^3P_1 \rightarrow {}^3F_3$	13605.71	53053.52	0.2565	18
	$^1D_2 \rightarrow {}^3H_4$	816.25	4636.94	0.176	215
BZLP: 2.5Pr	$^3P_1\ {}^3F_3$	13488.58	52998.95	0.2075	18
$^1D_2 \rightarrow {}^3H_4$		799.31	4589.27	0.1742	217

Table 5
Emission peak wavelength (λ_P)(nm), effective band widths ($\Delta\lambda_P$)(nm), measured and experimental branching ratios (β_R& β_{exp}), stimulated emission cross-sections (σ_{se}) (cm^2), gain band width ($\sigma_{se} \times \Delta\lambda_P$) ($cm^3$) and optical gain parameter ($\sigma_{se} \times \tau_R$) ($cm^2$ s) parameters for the emission transitions for Pr^{3+} ions in BZLP glasses.

Spectral parameters	BZLP:0.01Pr	BZLP:0.05Pr	BZLP:0.1Pr	BZLP:0.5Pr	BZLP:1.0Pr	BZLP:1.5Pr	BZLP:2.0 Pr	BZLP:2.5Pr
$^1D_2 \rightarrow {}^3H_4$								
λ_P	604	604	604	604	604	604	604	604
$\Delta\lambda$p	18.67	18.90	19.54	16.01	14.97	14.50	14.19	15.63
β_R	0.2479	0.2154	0.1806	0.1940	0.2146	0.2080	0.1760	0.1742
β_{exp}	0.88	0.94	0.95	0.37	0.48	0.45	0.56	0.39
σ_{se}	29.20	39.13	53.42	41.21	35.45	32.71	26.97	23.50
$\sigma_{se} \times \Delta\lambda_P$	54.54	73.98	104.41	66.00	53.07	47.45	38.30	36.74
$\sigma_{se} \times \tau_R$	7.39	6.10	4.80	6.18	7.05	6.77	5.79	5.10

and it is noticed that β_R values for high intense transition $^1D_2 \rightarrow {}^3H_4$ decreases as the concentration of Pr^{3+} ions increases up to 0.1 mol% and after that increases as the concentration increases up to 2.5 mol%. This might be due to fluorescent quenching of $^1D_2 \rightarrow {}^3H_4$ transition [26,32,46,48]. Moreover, higher value of stimulated emission cross-section (σ_{se} is essential for luminescent transition thereby showing that the glass can be used as an active medium for laser. From Tables 5 it is noticed that σ_{se} has maximum value for BZPL:0.1Pr glass for transition $^1D_2 \rightarrow {}^3H_4$ transition.

Furthermore, a glassy materials doped with rare earth ions having high values of gain bandwidth (σ_{se} x $\Delta\lambda$p) and optical gain parameters (σ_{se} x τ_R) can be used in construction of optical fibres. As is evident from Table 5, BZLP:0.1Pr glass has high values for all radiatitve parameters as compared to other reported glasses. Therefore, BZLP:0.1Pr i.e 0.1 mol% of Pr^{3+} doped BZLP glass is best fitted for reddish –orange laser transition at 604 nm.

3.5. Colorimetric study

Chromaticity color coordinates of Pr^{3+} doped BZLP glass samples were evaluated based on PL results at $\lambda_{ex} = 445$ nm and have been shown in Table 6. The estimated color coordinates lie in the red region of the CIE chromaticity diagram as shown in Fig. 9. Further, the color purity is one of the vital parameters stating how pure or monochromatic a light for utilization in photonic applications. The color purity (CP) for all the glass samples were calculated via using formula as mention in equation (11) [49,50]:

$$CP\ (\%) = \sqrt{\frac{(x - x_{ee})^2 + (y - y_{ee})^2}{(x_d - x_{ee})^2 + (y_d - y_{ee})^2}}\ x\ 100 \qquad (11)$$

here (x, y) indicates the estimated chromaticity color coordinates, (x_{ee}, y_{ee}) signify the standard white point coordinates (0.33, 0.33) and (x_d, y_d) is coordinates for the maximum wavelength. The calculated color purity for the optimized glass was found to be 98.61%. The highly pure color of the Pr^{3+} doped BZLP glass samples makes them an ideal candidate as a red light-emitting constituent in W-LEDs.

Table 6
CIE co-ordinates of Pr^{3+} ions in BZLP glasses.

Name of the sample	CIE co-ordinates	
	X co-ordinate	*Y* co-ordinate
BZLP: 0.01Pr	0.606	0.386
BZLP: 0.05Pr	0.628	0.363
BZLP: 0.1Pr	0.629	0.367
BZLP: 0.5Pr	0.571	0.416
BZLP: 1.0Pr	0.554	0.4231
BZLP: 1.5Pr	0.544	0.440
BZLP: 2.0 Pr	0.532	0.307
BZLP: 2.5 Pr	0.506	0.469

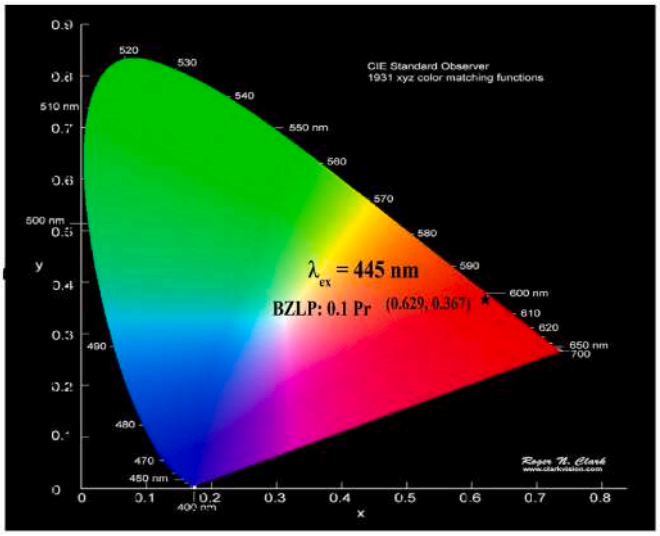

Fig. 9. CIE chromaticity coordinates of BZLP:0.10Pr glass.

3.6. PL decay analysis

PL decay profiles for Pr^{3+} doped BZLP glass samples have been documented at $\lambda_{ex} = 445$ nm and $\lambda_{em} = 604$ nm and shown in Fig. 10. The curves follow an exponential behaviour. The most proper fitting was attained for the bi-exponential function given by Ref. [51]:

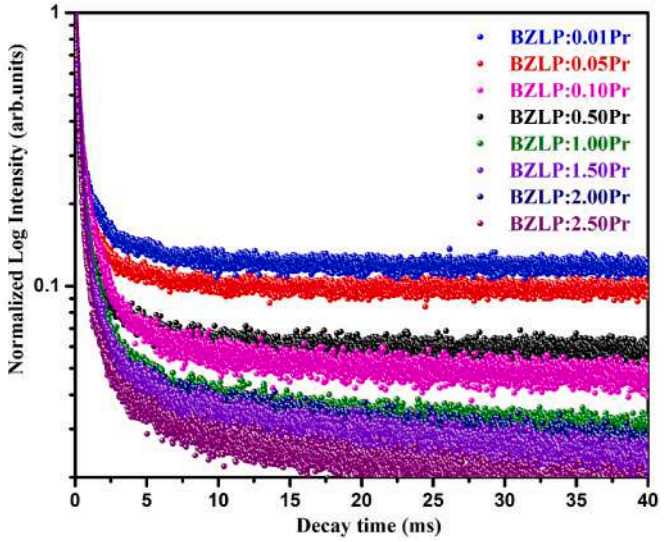

Fig. 10. PL decay curves of Pr^{3+} doped BZLP glasses with varying the doping concentration from 0.01 to 2.50 mol% under 445 nm excitation and emission at 604 nm.

$$I(t) = I_0 + A_1\ exp\left(-\frac{t}{\tau_1}\right) + A_2\ exp\left(-\frac{t}{\tau_2}\right) \quad (12)$$

here τ_1 and τ_2 symbolize slow and fast decay times in the exponential equation, respectively. Two fitting constants in equations designated by A_1 and A_2. $I(t)$ and I_0 are the emission intensities at time $= t$ sec and time $= 0$ s, respectively. The average (τ_{avg}) decay time for Pr^{3+} doped BZLP glass samples was assessed with the help of formula [16,52]:

$$\tau_{avg} = \frac{A_1{\tau_1}^2 + A_2{\tau_2}^2}{A_1\tau_1 + A_2\tau_2} \quad (13)$$

The τ_{avg} recorded decay profile of all glass samples was depicted in Table 7. The average decay time decreased with an increase of Pr^{3+} ions in the glass lattice. This is due to reduced distance between the Pr^{3+} ions thereby enhancing the non-radiative energy transfer. The estimated average decay time for BZLP:0.1Pr was $\tau_{avg} = 2.57$ ms which reduced to $\tau_{avg} = 1.23$ ms for BZLP:2.50 Pr glass. From Table 7 it is seen that τ_{exp} values are less than τ_R. This small variation between τ_{exp} and τ_R values arises due to multi phonon relaxation process. In this case τ_{exp} , τ_R and non-radiative decay rate (W_{NR}) are related as:

$$W_{NR} = \frac{1}{\tau_{exp}} - \frac{1}{\tau_R} \quad (14)$$

Table 7 contains the W_{NR} values determined using the aforementioned equation. Another crucial factor utilised to assess the luminescence intensity of reported glasses is the quantum efficiency (η %). By calculating the ratio between τ_{exp} and τ_R, quantum efficieny for prepared glasses has been estimated and presented in Table 7. It is evident from Table 7 that up to 0.1 mol% (BZLP:0.1Pr) glass, the value of η % rises and after that declines with increasing Pr^{3+} ions concentration. Furthermore, Table 8 represents the comparision between several radiative parameters with the other reported glasses in literature [44,53,54]. It has been observed that stimulated emission cross section of the Pr^{3+} BZLP doped glasses have larger value than other reported glasses [53,54] and are comparable with that of Pr^{3+} doped LiPbAlB glass reported by Nisha et al. [44]. From the data in Table 8, BZLP:0.1Pr glass had the best quantum efficiency and stimulated emission cross section as compared to other reported glasses. Therefore, under 445 nm excitation, BZLP:0.1Pr glass is most suited for lasing emission in the reddish orange region.

3.7. Temperature-dependent PL (TD-PL) characteristics

Thermal stability is one of the vital requirements of the luminescent materials for utility in W-LEDs. So, using the temperature dependent-photoluminescence (TD-PL) spectra, the thermal stability of the prepared glass samples was examined.The TD-PL spectra were reported at excitation wavelength of $\lambda_{ex} = 445$ nm as presented in Fig. 11. It is evident that with an increase in temperature from 300 K to 473 K, PL intensity diminishes gradually but the spectral shape/peak position is unaffected. Further, the activation energy (ΔE) was evaluated using the Arrhenius equation [55–57]:

Table 7
Experimental lifetime (τ_{exp}) (μs), radiative lifetime (τ_R) (μs), quantum efficiency (η), and non-radiative decay rates (W_{NR}) (s^{-1}) for Pr^{3+} ions in BZLP glasses.

Sample	τ_{exp} (μs)	τ_R (μs)	η (%)	W_{NR}
BZLP: 0.01Pr	91	253	35.96	7036
BZLP: 0.05Pr	89	156	57.05	4825
BZLP: 0.1Pr	87	90	96.66	383
BZLP: 0.5Pr	86	150	57.33	4961
BZLP: 1.0Pr	85	199	42.71	6739
BZLP: 1.5Pr	83	207	40.09	7217
BZLP: 2.0 Pr	80	215	37.20	7848
BZLP: 2.5 Pr	75	217	34.56	8725

Table 8
Comparison of emission characteristics parameters like effective band widths ($\Delta\lambda_P$)(nm), measured branching ratio (β_R) and stimulated emission cross-sections (σ_{se} x 10^{-22}) (cm^2) of transition $^1D_2 \rightarrow {}^3H_4$ in different Pr^{3+} doped glasses.

Name of the sample	$\Delta\lambda_P$	β_R	σ_{se}	η (%)	References
BZLP: 0.01Pr	18.67	0.2479	29.20	35.96	Present work
BZLP: 0.05Pr	18.90	0.2154	39.13	57.05	Present work
BZLP: 0.1Pr	19.54	0.1806	53.42	96.66	Present work
BZLP: 0.5Pr	16.01	0.1940	41.21	57.33	Present work
BZLP: 1.0Pr	14.97	0.2146	35.45	42.71	Present work
BZLP: 1.5Pr	14.50	0.2080	32.71	40.09	Present work
BZLP: 2.0 Pr	14.19	0.1760	26.97	37.20	Present work
BZLP: 2.5 Pr	15.63	0.1742	23.50	34.56	Present work
0.1 Pr:NaAlGdP	16.50	0.82	27.64	78	[53]
ZNBBP-1	26.48	0.34	16.49	–	[54]
LiPbAlBPr 1.0	18.09	0.41	46.1	86	[44]

$$I_T = \frac{I_0}{1 + C\ exp\left(-\frac{\Delta E}{K_B T}\right)} \quad (15)$$

In above expression I_0 and I_T indicate PL intensity at room temperature 300 K and at any temperature T (in Kelvin), respectively. K_B Symbolizes the Boltzmann constant and C is an arbitrary constant. The value of ΔE was assessed via the slope of the linear fitted plot between $ln((I_0/I_T)-1)$ and $1/K_BT$ as shown in Fig. 12 [49]. The activation energy was found to $\Delta E = 0.175$ eV for BZLP:0.1Pr glass. Inset plot of Fig. 12 reveals the PL intensity reduced from 88.12% at 423 K to 82.61% at 473 K, which shows that glass samples have brilliant thermal stability.

4. Conclusions

Trivalent praseodymium doped BZLP glass samples were synthesised through melt quenching route and their structural,physical and optical properties were studied for utility in luminescent device applications. The diffraction pattern confirmed the unstructured and nonexistent crystalline character of host glass. Absorption spectra showed several bands in ultraviolet, visible and infrared regions. The indirect optical bandgap was estimated using Tauc's plot for each glass and was found to be in the range 3.48–4.07 eV. Using J-O parameters derived from the absorption spectrum, several radiative parameters were assessed for the reported fluorescence peaks of Pr^{3+} ions in BZLP glass samples. The PL spectra at 445 nm excitation shows prominent emission peak at 604 nm due to $^1D_2 \rightarrow {}^3H_4$ transition of Pr^{3+} ions. Beyond 0.10 mol% of Pr^{3+} ion concentration, quenching effect is observed due to dipole-dipole type of interaction between the dopant ions as confirmed by the Dexter plot. For the stransition $^1D_2 \rightarrow {}^3H_4$, stimulated emission cross-section,branching ratios and quantum efficiency were assessed. The CIE coordinates for the as prepared glasses fall in deep-red region. The average lifetime values at $\lambda_{ex} = 445$ nm for 604 nm emission were observed to decrease with an increase in Pr^{3+} ion content in BZLP glasses. The TD-PL study shows that the glass has an excellent thermal stability with activation energy $\Delta E = 0.175$ eV. After analysing the several evaluated radiative parameters, it was revealed that amongst all the Pr^{3+} doped BZLP glass samples, BZLP:0.1Pr glass can be used as a deep red-emitting component in blue pumped white LED and other luminescent device applications.

CRediT authorship contribution statement

Kartika Maheshwari: Writing, experimentation, Conceptualization, synthesis of samples. **Ravita:** Formal analysis. **Aman Prasad:** Formal analysis, editing, writing. **Yasha Tayal:** Formal analysis. **A.S. Rao:** Supervision, Writing – review and editing.

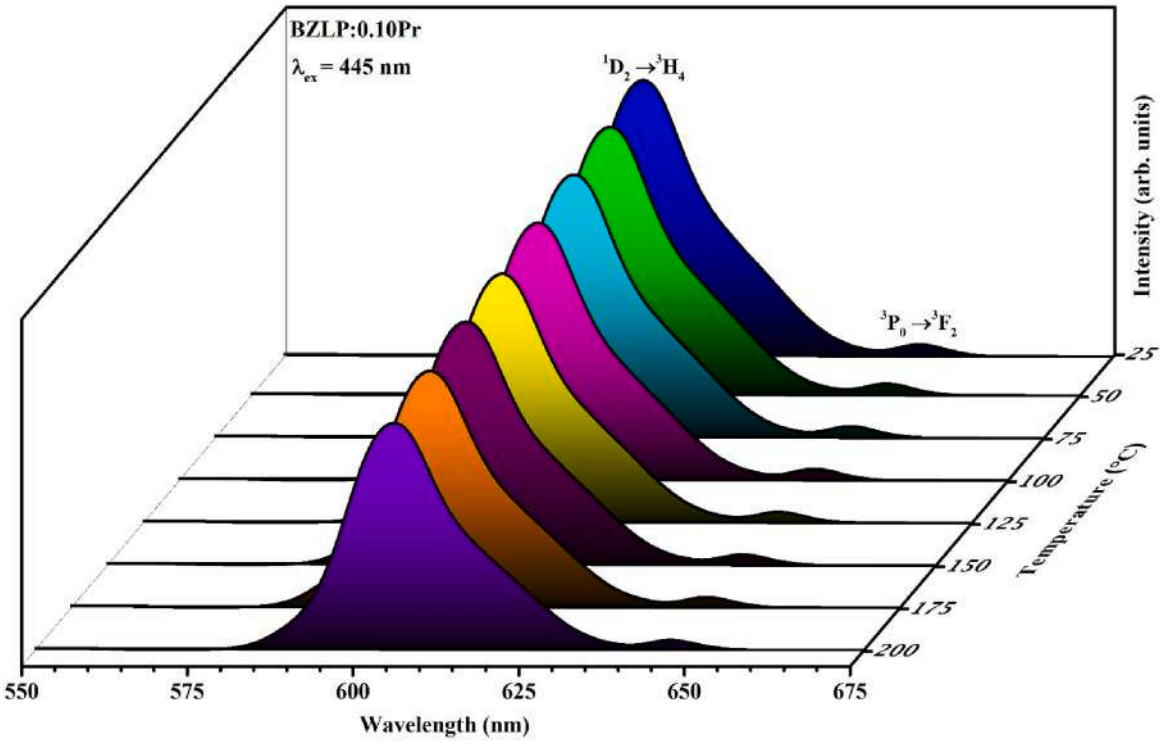

Fig. 11. TD-PL spectra of optimized BZLP:0.10Pr glass with temperature varying from 27 °C to 200 °C under 445 nm excitation wavelength.

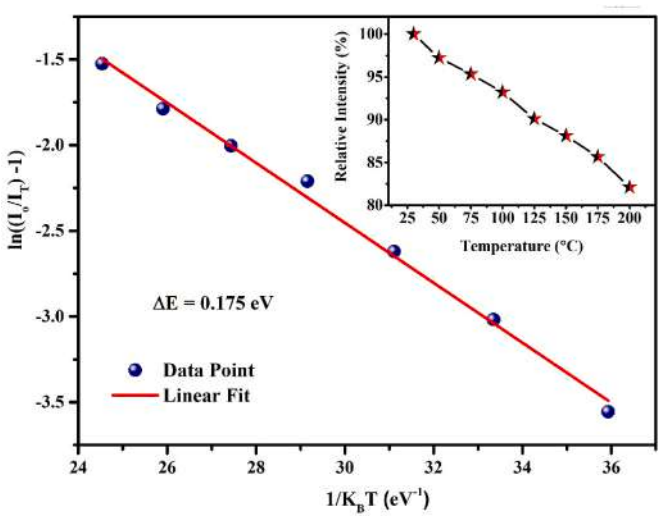

Fig. 12. Graph between $\ln[(I_o/I_T)-1]$ and $(1/K_BT)$ for BZLP:0.10Pr glass. The inset plot shows the decrease in relative emission intensity with rise in temperature from 27 °C to 200 °C.

Declaration of competing interest

The authors declare that they have no known competing financial interests or personal relationships that could have appeared to influence the work reported in this paper.

Data availability

The authors do not have permission to share data.

Acknowledgments

The authors are thankful to Delhi Technological University, Delhi for providing the necessary infrastructure and a conducive work environment to perform this research.

References

[1] A.S. Rao Ravita, Effective energy transfer from Dy^{3+} to Tb^{3+} ions in thermally stable KZABS glasses for intense green emitting device applications, J. Lumin. 239 (2021), 118325, https://doi.org/10.1016/j.jlumin.2021.118325.

[2] T.H. Kim, W. Wang, Q. Li, Advancement in materials for energy-saving lighting devices, Front. Chem. Sci. Eng. 6 (2012) 13–26, https://doi.org/10.1007/s11705-011-1168-y.

[3] X. Chen, P. Dai, X. Zhang, C. Li, S. Lu, X. Wang, Y. Jia, Y. Liu, Phosphor via dual energy transfers for white light-emitting diodes, Inorg. Chem. 53 (2014) 3441–3448.

[4] R.J. Xie, N. Hirosaki, N. Kimura, K. Sakuma, M. Mitomo, 2-Phosphor-Converted white light-emitting diodes using oxynitride/nitride phosphors, Appl. Phys. Lett. 90 (2007), 191101, https://doi.org/10.1063/1.2737375.

[5] J. Chen, Y. Liu, L. Mei, H. Liu, M. Fang, Z. Huang, Crystal structure and temperature-dependent luminescence characteristics of $KMg_4(PO_4)_3:Eu^{(2+)}$ phosphor for white light-emitting diodes, Sci. Rep. 5 (2015) 9673, https://doi.org/10.1038/srep09673.

[6] S.M. Rafiaei, A. Bahrami, The effects of boric acid on crystal structure, nano-/microstructure and photoluminescence characteristics of rare earth-doped Y_2O_3/YBO_3 composite compounds, J. Nanostructure Chem. 7 (2017) 367–373, https://doi.org/10.1007/s40097-017-0246-1.

[7] N. Deopa, A.S. Rao, Photoluminescence and energy transfer studies of Dy^{3+} ions doped lithium lead alumino borate glasses for w-LED and laser applications, J. Lumin. 192 (2017) 832–841, https://doi.org/10.1016/j.jlumin.2017.07.052.

[8] N. Deopa, A.S. Rao, Spectroscopic studies of Sm^{3+} ions activated lithium lead alumino borate glasses for visible luminescent device applications, Opt. Mater. 72 (2017) 31–39, https://doi.org/10.1016/j.optmat.2017.04.067.

[9] R.A. Talewar, S. Mahamuda, K. Swapna, A.S. Rao, Sensitization of Yb^{3+} by Nd^{3+} emission in alkaline-earth chloro borate glasses for laser and fiber amplifier applications, J. Alloys Compd. 771 (2019) 980–986, https://doi.org/10.1016/j.jallcom.2018.08.270.

[10] K. Jha, M. Jayasimhadri, D. Haranath, K. Jang, Influence of modifier oxides on spectroscopic properties of Eu $^{3+}$ doped oxy-fluoro tellurophosphate glasses for visible photonic applications, J. Alloys Compd. 789 (2019) 622–629, https://doi.org/10.1016/j.jallcom.2019.02.277.

[11] J. Gou, J. Fan, S. Zuo, M. Luo, Y. Chen, X. Zhou, Y. Yang, B. Yu, S.F. Liu, Highly thermally stable and emission color tunable borate glass for white-light-emitting

diodes with zero organic resin, J. Am. Ceram. Soc. 100 (2017) 4011–4020, https://doi.org/10.1111/jace.14951.
[12] M. Jayasimhadri, K. Jang, H.S. Lee, B. Chen, S.S. Yi, J.H. Jeong, White light generation from Dy^{3+} -doped ZnO- B_2O_3 - P_2O_5 glasses, J. Appl. Phys. 106 (2009), https://doi.org/10.1063/1.3159899.
[13] K. Maheshwari, A.S. Rao, Photoluminescence downshifting studies of thermally stable Dy^{3+} ions doped phosphate glasses for photonic device applications, Opt. Mater. 129 (2022), 112518, https://doi.org/10.1016/J.OPTMAT.2022.112518.
[14] K. Jha, M. Jayasimhadri, Structural and emission properties of Eu^{3+} -doped alkaline earth zinc - phosphate glasses for white LED applications, J. Am. Ceram. Soc. (2017) 1402–1411, https://doi.org/10.1111/jace.14668.
[15] C. Zuo, Z. Zhou, L. Zhu, A. Xiao, Y. Chen, X. Zhang, X. Ding, Q. Ge, Spectroscopic properties of Ce^{3+}-doped borosilicate glasses under UV excitation, Mater. Res. Bull. 83 (2016) 155–159, https://doi.org/10.1016/j.materresbull.2016.06.001.
[16] N. Deopa, B. Kumar, M.K. Sahu, P.R. Rani, A.S. Rao, Effect of Sm^{3+} ions concentration on borosilicate glasses for reddish orange luminescent device applications, J. Non-Cryst. Solids 513 (2019) 152–158, https://doi.org/10.1016/j.jnoncrysol.2019.03.025.
[17] M. Kumar, A.S. Rao, Concentration-dependent reddish-orange photoluminescence studies of Sm^{3+} ions in borosilicate glasses, Opt. Mater. 109 (2020), 110356, https://doi.org/10.1016/j.optmat.2020.110356.
[18] C.B. Annapurna Devi, S. Mahamuda, M. Venkateswarlu, K. Swapna, A. Srinivasa Rao, G. Vijaya Prakash, Dy^{3+} ions doped single and mixed alkali fluoro tungsten tellurite glasses for Laser and white LED applications, Opt. Mater. 62 (2016) 569–577, https://doi.org/10.1016/j.optmat.2016.11.016.
[19] Ravita, A. Prasad, P. Rohilla, A. Shandilya, A.S. Rao, Photoluminescence and energy transfer studies on Tm^{3+}/Dy^{3+}/Eu^{3+}doped borosilicate glasses for color tunability and warm white light generation, J. Non-Cryst. Solids 606 (2023) 122192, doi:10.1016/j.jnoncrysol.2023.122192.
[20] W. Hordijk, G. Blasse, Energy transfer by sensitizer-activator pairing in calcium sulphate, J. Lumin. 6 (1973) 137–139, https://doi.org/10.1016/0022-2313(73)90050-1.
[21] K.R. Vighnesh, B. Ramya, S. Nimitha, A. Wagh, M.I. Sayyed, E. Sakar, H.A. Yakout, A. Dahshan, S.D. Kamath, Structural, optical, thermal, mechanical, morphological & radiation shielding parameters of Pr^{3+} doped ZAlFB glass systems, Opt. Mater. 99 (2020), 109512, https://doi.org/10.1016/j.optmat.2019.109512.
[22] C.Y. Morassuti, L.H.C. Andrade, J.R. Silva, M.L. Baesso, F.B. Guimarães, J. H. Rohling, L.A.O. Nunes, G. Boulon, Y. Guyot, S.M. Lima, Spectroscopic investigation and interest of Pr^{3+} -doped calcium aluminosilicate glass, J. Lumin. 210 (2019) 376–382, https://doi.org/10.1016/j.jlumin.2019.02.051.
[23] D. Manzani, D. Pabœuf, S.J.L. Ribeiro, P. Goldner, F. Bretenaker, Orange emission in Pr^{3+}-doped fluoroindate glasses, Opt. Mater. 35 (2013) 383–386, https://doi.org/10.1016/j.optmat.2012.09.030.
[24] Ravita, A. S.Rao, Effective sensitization of Eu^{3+} visible red emission by Sm^{3+} in thermally stable potassium zinc alumino borosilicate glasses for photonic device applications, J. Lumin. (2021) 118689, doi:10.1016/j.jlumin.2021.118689.
[25] P.P. Pawar, S.R. Munishwar, R.S. Gedam, Physical and optical properties of Dy^{3+}/Pr^{3+} Co-doped lithium borate glasses for W-LED, J. Alloys Compd. 660 (2016) 347–355, https://doi.org/10.1016/J.JALLCOM.2015.11.087.
[26] S. Mahamuda, K. Swapna, A. Srinivasa Rao, T. Sasikala, L. Rama Moorthy, Reddish-orange emission from Pr^{3+} doped zinc alumino bismuth borate glasses, Phys. B Condens. Matter 428 (2013) 36–42, https://doi.org/10.1016/j.physb.2013.07.010.
[27] W.T. Carnall, P.R. Fields, K. Rajnak, Electronic energy levels of the trivalent lanthanide aquo ions. I. Pr^{3+}, Nd^{3+}, Pm^{3+}, Sm^{3+}, Dy^{3+}, Ho^{3+}, Er^{3+} and Tm^{3+}, J. Chem. Phys. 49 (1968) 4424–4442, https://doi.org/10.1063/1.1669893.
[28] T.H.S. Tanabe, T. Ohyagi, N. Soga, Compositional dependence of judd-ofelt parameters of Er^{3+} ions in alkali- metal borate glasses, Phys. Rev. B 46 (2018) 3305, https://doi.org/10.1103/PhysRevB.46.3305.
[29] M.B. Saisudha, J. Ramakrishna, Optical absorption of Nd $^{3+}$, Sm $^{3+}$ and Dy $^{3+}$ in bismuth borate glasses with large radiative transition probabilities, Opt. Mater. 18 (2002) 403–441, https://doi.org/10.1016/S0925-3467(01)00181-1.
[30] S. Mahamuda, K. Swapna, M. Venkateswarlu, A.S. Rao, S.L. Shakya, G.V. Prakash, Spectral characterization of Sm^{3+} ions doped oxy-fluoroborate glasses for visible orange luminescent applications, J. Lumin. (2014), https://doi.org/10.1016/j.jlumin.2014.05.017.
[31] P Nemec, M. Frumar, Synthesis and properties of Pr $^{3+}$ -doped Ge – Ga – Se glasses, J. Non-Cryst. Solids 302 (2002) 1018–1022, https://doi.org/10.1016/S0022-3093(01)01127-9.
[32] M. Venkateswarlu, M.V.V.K.S. Prasad, K. Swapna, S. Mahamuda, Pr $^{3+}$ doped lead tungsten tellurite glasses for visible red lasers, Ceram. Int. 40 (2014) 6261–6269, https://doi.org/10.1016/j.ceramint.2013.11.084.
[33] C.B. Annapurna, S. Mahamuda, K. Swapna, M. Venkateswarlu, A.S. Rao, G. V. Prakash, Pr^{3+} ions doped single alkali and mixed alkali fluoro tungsten tellurite glasses for visible red luminescent devices, J. Non-Cryst. Solids 498 (2018) 345–351, https://doi.org/10.1016/j.jnoncrysol.2018.03.034.
[34] L. Sojka, Z. Tang, D. Furniss, H. Sakr, A. Oladeji, E.B. Pawlik, H. Dantanarayana, E. Faber, A.B. Seddon, T.M. Benson, S. Sujecki, Broadband, mid-infrared emission from Pr^{3+} doped GeAsGaSe chalcogenide fiber, optically clad, Opt. Mater. 36 (2014) 1076–1082, https://doi.org/10.1016/j.optmat.2014.01.038.
[35] M. Czaja, Optical properties of Pr^{3+} , Sm^{3+} and Er^{3+} doped P $_2$O $_5$ – CaO – SrO – BaO phosphate glass, Opt. Mater. 32 (2010) 547–553, https://doi.org/10.1016/j.optmat.2009.11.011.
[36] M.A. Newhouse, R.F. Bartholomew, B.G. Aitken, L.J. Button, N.F. Borrelli,Pr-doped mixed-halide glasses for 1300 nm amplification, IEEE Photon. Technol. Lett. 6 (1994) 189–191.
[37] I. Pal, A. Agarwal, S. Sanghi, M.P. Aggarwal, Structural , absorption and fluorescence spectral analysis of Pr3+ ions doped zinc bismuth borate glasses 509 (2011) 7625–7631, https://doi.org/10.1016/j.jallcom.2011.04.114.
[38] M. Vijayakumar, K. Marimuthu, Structural and luminescence properties of Dy^{3+} doped oxyfluoro-borophosphate glasses for lasing materials and white LEDs, J. Alloys Compd. 629 (2015) 230–241, https://doi.org/10.1016/j.jallcom.2014.12.214.
[39] V.H. Rao, P.S. Prasad, K.S. Babu, Visible luminescence characteristics of Pr $^{3+}$ ions in TeO $_2$ – Sb $_2$O $_3$ – WO_3 glasses, Opt. Mater. 101 (2020), 109740, https://doi.org/10.1016/j.optmat.2020.109740.
[40] K. Jha, M. Jayasimhadri, Spectroscopic investigation on thermally stable Dy^{3+} doped zinc phosphate glass for white light emitting diodes, J. Alloys Compd. 688 (2016) 833–840, https://doi.org/10.1016/j.jallcom.2016.07.024.
[41] M. So, A. Górny, L. Zur, M. Ferrari, G.C. Righini, W.A. Pisarski, J. Pisarska, White light emission through energy transfer processes in barium gallo- germanate glasses co-doped with Dy $^{3+}$ -Ln $^{3+}$ (Ln = Ce , Tm), Opt. Mater. 87 (2019) 63–69, https://doi.org/10.1016/j.optmat.2018.05.071.
[42] H.H. Caspers, H.E. Rast, R.A. Buchanan, Energy levels of Pr^{3+} in LaF_3, J. Chem. Phys. 43 (1965) 2124, https://doi.org/10.1063/1.1697083.
[43] P. Ramakrishna, R.K. Padhi, S. Kumar, D.K. Mohapatra, H. Jena, B.S. Panigrahi, Effect of U on the photoluminescence of Pr and structural properties of U/Pr doped and co-doped Li $_2$ O – ZnO – SrO borophosphate glass, Opt. Mater. 134 (2022), 113121, https://doi.org/10.1016/j.optmat.2022.113121.
[44] N. Deopa, A.S. Rao, S. Mahamuda, M. Gupta, M. Jayasimhadri, D. Haranath, G. V. Prakash, Spectroscopic studies of Pr^{3+} doped lithium lead alumino borate glasses for visible reddish orange luminescent device applications, J. Alloys Compd. 708 (2017) 911–921, https://doi.org/10.1016/j.jallcom.2017.03.020.
[45] Y. Tayal, A.S. Rao, Spectroscopic analysis of Dy^{3+} ions activated borosilicate glasses for photonic device applications, Opt. Mater. 117 (2021), 111112, https://doi.org/10.1016/j.optmat.2021.111112.
[46] D.V.R. Murthy, B.C. Jamalaiah, T. Sasikala, L. Rama Moorthy, M. Jayasimhadri, K. Jang, H.S. Lee, S.S. Yi, J.H. Jeong, Optical absorption and emission characteristics of Pr^{3+}-doped RTP glasses, Phys. B Condens. Matter 405 (2010) 1095–1100, https://doi.org/10.1016/J.PHYSB.2009.11.012.
[47] P. Karthikeyan, R. Vijayakumar, K. Marimuthu, Luminescence studies on Dy^{3+} doped calcium boro-tellurite glasses for White light applications, Phys. B Condens. Matter 521 (2017) 347–354, https://doi.org/10.1016/j.physb.2017.07.018.
[48] G. Lakshminarayana, K.M. Kaky, S.O. Baki, S. Ye, A. Lira, I.V. Kityk, M.A. Mahdi, Concentration dependent structural, thermal, and optical features of Pr^{3+}-doped multicomponent tellurite glasses, J. Alloys Compd. 686 (2016) 769–784, https://doi.org/10.1016/j.jallcom.2016.06.069.
[49] G. Zhu, Z. Li, C. Wang, X. Wang, F. Zhou, M. Gao, S. Xin, Y. Wang, Highly Eu $^{3+}$ ions doped novel red emission solid solution phosphors Ca $_{18}$ Li $_3$ (Bi,Eu)(PO $_4$) $_{14}$: structure design, characteristic luminescence and abnormal thermal quenching behavior investigation, Dalton Trans. 48 (2019) 1624–1632, https://doi.org/10.1039/c8dt04047h.
[50] G. Swati, S. Bishnoi, P. Singh, N. Lohia, V.V. Jaiswal, M.K. Dalai, D. Haranath, Chemistry of extracting high-contrast invisible fingerprints from transparent and colored substrates using a novel phosphorescent label, Anal. Methods 10 (2018) 308–313, https://doi.org/10.1039/c7ay02713c.
[51] V. Naresh, B.S. Ham, Influence of multiphonon and cross relaxations on $^3P_0$ and $^1D_2$ emission levels of Pr^{3+} doped borosilicate glasses for broad band signal amplification, J. Alloys Compd. 664 (2016) 321–330, https://doi.org/10.1016/j.jallcom.2015.12.246.
[52] Y. Wang, W. Zheng, Y. Lu, P. Li, S. Xu, J. Zhang, Effect of alkaline earth metals on luminescence characteristic in Eu-Doped oxynitride phosphate glasses, J. Lumin. 237 (2021), 118152, https://doi.org/10.1016/j.jlumin.2021.118152.
[53] N. Wantana, E. Kaewnuam, N. Chanthima, H.J. Kim, J. Kaewkhao, Optik Tuneable Luminescence of Pr $^{3+}$ -doped Sodium Aluminium Gadolinium Phosphate Glasses for Photonics Applications, 2022, p. 267, https://doi.org/10.1016/j.ijleo.2022.169668.
[54] V. Hegde, C.S.D. Viswanath, N. Chauhan, K.K. Mahato, S.D. Kamath, Photoluminescence and thermally stimulated luminescence properties of Pr^{3+} -doped zinc sodium bismuth borate glasses, Opt. Mater. 84 (2018) 268–277, https://doi.org/10.1016/j.optmat.2018.06.064.
[55] U. Farooq, Z. Zhao, Z. Sui, C. Gao, R. Dai, Z. Wang, Z. Zhang, Tm^{3+}/Dy^{3+}/Eu^{3+} (Sm^{3+}) tri-activated Y_2WO_6 as one potential single-phase phosphor for WLEDs, J. Alloys Compd. 778 (2019) 942–950, https://doi.org/10.1016/j.jallcom.2018.11.091.
[56] K. Maheshwari, A.S. Rao, Down-shifting photoluminescent properties of Tb^{3+} doped phosphate glasses for intense green-emitting devices applications, Opt. Mater. 137 (2023), 113533, https://doi.org/10.1016/j.optmat.2023.113533%0A.
[57] Ravita, A. S. Rao, Tunable photoluminescence studies of KZABS: RE $^{3+}$ (RE $^{3+}$ = Tm $^{3+}$, Tb $^{3+}$ and Sm $^{3+}$) glasses for w-LEDs based on energy transfer, J. Lumin. 251 (2022) 119194, doi:10.1016/j.jlumin.2022.119194.